NJC

PAPER

View Article Online
View Journal

Cite this: DOI: 10.1039/c5nj03347k

The first example of cofacial bis(dipyrrins)†

Jude Deschamps,[a] Yi Chang,[b] Adam Langlois,[a] Nicolas Desbois,[b] Claude P. Gros*[b] and Pierre D. Harvey*[a]

Received (in Montpellier, France) 26th November 2015, Accepted 21st March 2016

DOI: 10.1039/c5nj03347k

www.rsc.org/njc

Two series of cofacial bis(dipyrrins) were prepared and their photophysical properties as well as their bimolecular fluorescence quenching with C_{60} were investigated. DFT and TDDFT computations were also performed as a modeling tool to address the nature of the fluorescence state and the possible inter-chromophore interactions. Clearly, there is no evidence for such interactions and the bimolecular quenching of fluorescence, in comparison with mono-dipyrrins, indicates that C_{60}-bis(dipyrrin) contacts occur from the outside of the "mouth" of the cofacial structure.

Introduction

The generally strongly fluorescent dipyrrins are BODIPY-type dyes structurally related to porphyrins (Fig. 1).[1–4] They have been investigated due to their ability to form metal complexes,[5–7] and more recently the construction of bis(dipyrrin)s was performed and reviewed.[8] However, investigation of bis(dipyrrins) placed in a cofacial fashion was never reported. For instance, upon placing two porphyrin units in a cofacial fashion, it is well known that inter-ring interactions, as those shown in Fig. 1, lead to expected modifications of the optical properties,[9,10] and more recently provided valuable models for the special pairs.[11–13]

In the cofacial bis(porphyrin) compounds listed in Fig. 1, the C_{meso}–C_{meso} distance (*meso* carbons directly linked to the spacer) varied as 3.80 (DPB), 4.32 (DPX), 4.94 (DPA), 5.53 (DPO), and 6.32 Å (DPS),[14] and there is an obvious gradual progression of the photophysical parameters (fluorescence lifetimes and quantum yields, non-radiative and radiative rate constants,[15] and the rate of singlet and triplet energy transfer)[16] of the cofacially placed free-base porphyrins with the distance.

However, for cofacial bis(dipyrrins) systems using the classic boron-center, the tetrahedral geometry of this atom intuitively induces obvious steric hindrance preventing strong π-interactions between the pyrrole groups. We now report the synthesis and photophysical characterization in order to address this point, and indeed the two isolated dipyrrin units almost act as if they are independent (Fig. 2).

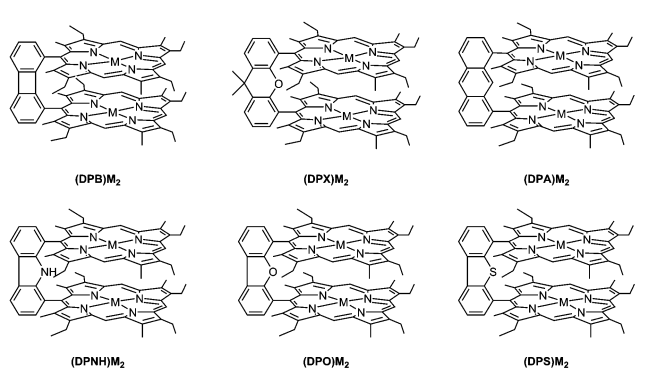

Fig. 1 Structures of the cofacial bisporphyrins recently investigated (M = 2H, transition metal).

[a] Département de Chimie, Université de Sherbrooke, Sherbrooke, Québec, J1K 2R1, Canada. E-mail: Pierre.Harvey@USherbrooke.ca
[b] ICMUB (UMR CNRS 6302), Université de Bourgogne Franche-Comté, 21 000 Dijon, France. E-mail: Claude.Gros@u-bourgogne.fr

† Electronic supplementary information (ESI) available. See DOI: 10.1039/c5nj03347k

Experimental

Experimental section

Materials. The handling of all air/water sensitive materials was carried out using standard techniques. DCM was distilled from CaH_2. Unless specified otherwise all other solvents were used as commercially supplied. Where mixtures of solvents were used, ratios are reported by volume. Column chromatography was carried out on silica gel 60 at normal pressure. For photophysical measurements, all chemicals were of analytical reagent quality and were used as received. THF was distilled over Na/benzophenone and 2-MeTHF filtrated over alumina, and then distilled under an inert atmosphere using CaH_2 as a drying agent. Dry 2-MeTHF was degassed in a sonic bath by repeated cycles of vacuum and purging with argon, and then stored inside a glove box under an almost oxygen-free argon atmosphere (O_2 levels less than 10 ppm). Anhydrous 1,2-dichlorobenzene (Sigma-Aldrich) was used without any further drying, but was degassed and stored in the same manner as the 2-MeTHF.

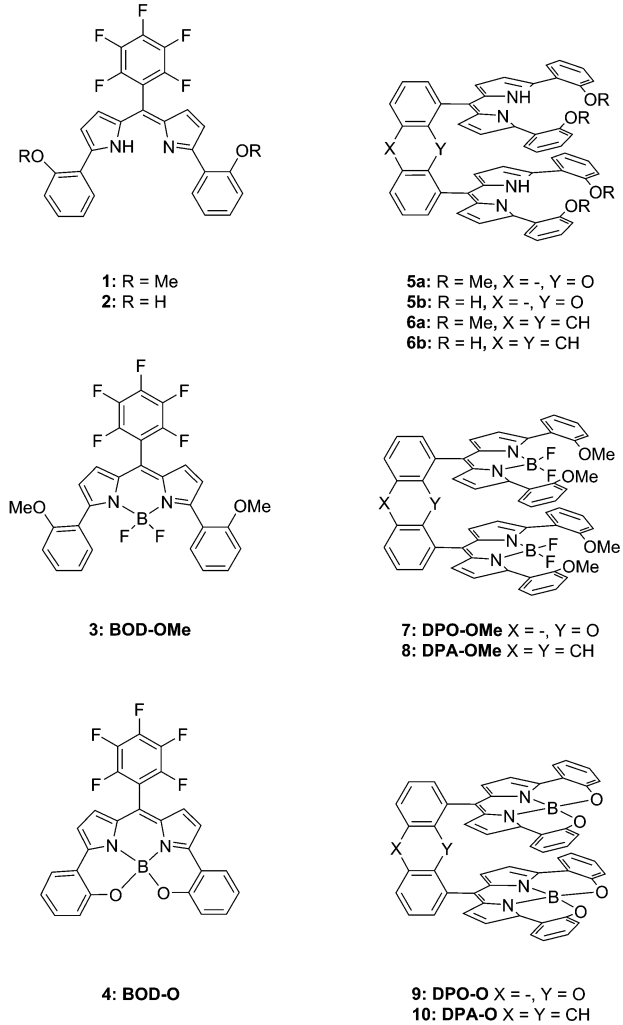

Fig. 2 Structures of the investigated mono- and bis(dipyrrins).

Synthesis

Dipyrrin-OMe (1). To a stirred solution containing 2-(2-methoxyphenyl)pyrrole (0.82 g, 4.74 mmol, 1.0 eq.) and pentafluorobenzaldehyde (0.42 g, 2.14 mmol, 0.5 eq.) in CH_2Cl_2 (40 mL), trifluoroacetic acid (60 μL) was added under an argon atmosphere and the mixture was stirred for 2 h at room temperature. 2,3-Dichloro-5,6-dicyano-1,4-benzoquinone (DDQ, 0.55 g, 2.42 mmol) was added and the resulting solution was stirred overnight at rt. The reaction mixture was washed with saturated $NaHCO_3$ aqueous solution, extracted with CH_2Cl_2, dried over $MgSO_4$, and concentrated to a small volume that was loaded directly on a short alumina pad. The filtrate was evaporated to dryness, taken in the minimum amount of CH_2Cl_2 and purified over a silica gel column, using a 8 : 2 : 0.01 mixture of CH_2Cl_2/EtOAc/NEt_3 as a solvent (golden brown solid; 0.96 g, 77%). ^{1}H NMR ($CDCl_3$, 300 MHz) δ 8.03 (dd, 2H), 7.34 (ddd, 2H), 7.02 (m, 4H), 6.94 (d, 2H), 6.47 (d, 2H), 3.87 (s, 6H). ^{13}C NMR ($CDCl_3$, 75 MHz) δ 157.4, 153.9, 140.3, 130.3, 129.1, 126.5, 121.9, 120.9, 119.6, 111.6, 55.9, 26.9. MALDI-TOF MS: *m*/*z* calcd for $C_{29}H_{19}F_5N_2O_2$: 522.1367; found: 522.883. Anal. calcd for $C_{29}H_{19}F_5N_2O_2$: C, 66.67; H, 3.67; N, 5.36. Found: C, 66.85; H, 4.38; N, 5.03.

BOD-OMe (3). To a stirred solution containing dipyrrin-OMe (**1**) (0.1 g, 0.19 mmol) in CH_2Cl_2 (15 mL), was added triethylamine (100 μL) and the mixture was stirred for 5 min at room temperature. BF_3 (48%, 150 μL) was added and the resulting solution was stirred for 3 h at rt. The reaction mixture was washed with saturated $NaHCO_3$ aqueous solution, dried over $MgSO_4$, and concentrated to a small volume that was loaded directly on a silica gel column, using CH_2Cl_2 as the solvent. The purple fraction was collected to yield the pure compound. **BOD-OMe (3)** (purple solid; 85 mg, 74%). ^{1}H NMR ($CDCl_3$, 300 MHz) δ 7.78 (dd, 2H), 7.40–7.32 (m, 2H), 7.01 (m, 2H), 6.95–6.93 (d, 1H), 6.91 (d, 1H), 6.70 (d, 2H), 6.65 (d, 2H), 3.79 (s, 6H). ^{13}C NMR ($CDCl_3$, 75 MHz) δ 157.7, 135.2, 131.9, 131.1, 127.8, 126.4, 123.6, 121.5, 120.3, 111.0, 55.8. ESI-HRMS: *m*/*z* calcd for $C_{29}H_{18}B_1F_7N_2O_2Na^+$: 593.12469; found: 593.12286. UV-vis λ_{max} (CH_2Cl_2)/nm 565 (ε/dm^3 mol^{-1} cm^{-1} 11 000), 344 (2400). Anal. calcd for $C_{29}H_{18}BF_7N_2O_2$: C, 61.08; H, 3.18; N, 4.91. Found: C, 61.69; H, 3.60; N, 5.13.

BOD-O (4). The experimental procedure was adapted from the methodology described in the literature for the preparation of the phenyl analog. To a stirred solution of **BOD-OMe (3)** (0.4 g, 0.72 mmol) in CH_2Cl_2 (12 mL), BBr_3 (0.68 mL, 7.2 mmol) was added at 0 °C under an argon atmosphere. The reaction mixture was stirred and allowed to warm up to room temperature and left for 3 days before quenching with methanol. The mixture was evaporated and dissolved again with methanol. To the resulting mixture, conc. HCl (37%) was added and the reaction mixture was heated under reflux for 3 h. After cooling, the mixture was neutralized with a saturated $NaHCO_3$ aqueous solution and extracted with ethylacetate. The organic layer was dried over $MgSO_4$, evaporated to dryness and purified by column chromatography using a 1 : 1 mixture of CH_2Cl_2/heptane as the solvent. The expected compound (**2**) was isolated as a dark purple solid (0.12 g, 32%).

The product above was directly used for the next step reaction. To a stirred solution containing (**2**) (30 mg, 0.06 mmol) in 5 mL of $CHCl_3$ was added $B(OMe)_3$ (100 μL). The reaction mixture was heated under reflux for 4 h. After cooling, the mixture was evaporated to dryness and the residue was purified by column chromatography on silica gel using hexane–CH_2Cl_2 (1 : 1) as the solvent, and recrystallized from CH_2Cl_2/MeOH to give **BOD-O (4)** (25 mg, 83%). ^{1}H NMR ($CDCl_3$, 300 MHz) δ 7.80 (dd, 2H), 7.38 (m, 2H), 7.08 (m, 2H), 6.99 (dd, 2H), 6.94 (s, 4H). ^{13}C NMR ($CDCl_3$, 75 MHz) δ 154.4, 151.7, 134.6, 132.9, 127.8, 126.1, 120.7, 119.9, 119.3, 117.1. MALDI-TOF MS: *m*/*z* calcd for $C_{27}H_{12}BF_5N_2O_2$: 502.0912; found: 502.791. Anal. calcd for $C_{27}H_{12}BF_5N_2O_2$: C, 64.57; H, 2.41; N, 5.58. Found: C, 64.32; H, 3.34; N, 5.24.

4,6-Bis((*Z*)-(5-(2-methoxyphenyl)-1*H*-pyrrol-2-yl)(5-(2-methoxyphenyl)-2*H*-pyrrol-2-ylidene)methyl) dibenzo[*b*,*d*]furan (5a). Dibenzo[*b*,*d*]furan-4,6-dicarbaldehyde (173 mg, 0.77 mmol) and 2-(2-methoxyphenyl)-1*H*-pyrrole (500 mg, 2.9 mmol) were dissolved in dry CH_2Cl_2 (80 mL) under an argon atmosphere. Trifluoroacetic acid (TFA, 75 μL) was added, and the solution was stirred for 3 h at room temperature in the dark (until TLC indicated complete consumption of the aldehyde). 2,3-Dichloro-5,6-dicyanoquinone

(DDQ, 300 mg, 1.3 mmol) was added, and the mixture was stirred for an additional 4 h. The reaction mixture was washed twice with water and brine, dried over $MgSO_4$, and concentrated at reduced pressure. The crude product was firstly purified by alumina and further purification by silica-gel column chromatography (dichloromethane/ethyl acetate: 4/1) was used to get the red solid. Compound **5a** (red solid; 150 mg, 22% yield). ^{1}H NMR ($CDCl_3$, 300 MHz) δ 13.47 (s, 2H), 8.11 (dd, 2H), 7.86 (dd, 4H), 7.58 (dd, 2H), 7.45 (t, 2H), 7.25–7.20 (m, 4H), 6.88 (t, 8H), 6.75 (d, 4H), 6.44 (d, 4H), 3.72 (s, 12H). ^{13}C NMR ($CDCl_3$, 75 MHz) δ 157.3, 154.6, 152.2, 140.8, 132.8, 130.5, 129.2, 129.0, 128.2, 124.2, 122.7, 122.2, 120.7, 118.4, 111.5, 55.8. HRMS (MALDI-TOF): *m*/*z* calcd for $C_{58}H_{45}N_4O_5$: 877.3384; found: 877.3393 $[M + H]^+$. Anal. calcd for $C_{58}H_{44}N_4O_5$: C, 79.43; H, 5.06; N, 6.39. Found: C, 79.44; H, 5.08; N, 6.21.

1,8-Bis((*Z*)-(5-(2-methoxyphenyl)-1*H*-pyrrol-2-yl)(5-(2-methoxyphenyl)-2*H*-pyrrol-2-ylidene)methyl) anthracene (6a). Anthracene-1,8-dicarbaldehyde (200 mg, 0.85 mmol) and 2-(2-methoxyphenyl)-1*H*-pyrrole (600 mg, 3.5 mmol) were dissolved in dry CH_2Cl_2 (100 mL) under an argon atmosphere. Trifluoroacetic acid (TFA, 90 μL) was added, and the solution was stirred for 3 h at room temperature in the dark (until TLC indicated complete consumption of the aldehyde). 2,3-Dichloro-5,6-dicyanoquinone (DDQ, 350 mg, 1.5 mmol) was added, and the mixture was stirred for an additional 12 h. The reaction mixture was washed twice with water and brine, dried over $MgSO_4$, and concentrated at reduced pressure. The crude product was firstly purified by alumina and further purification by silica-gel column chromatography (dichloromethane/ethyl acetate: 3/1) was used to get the red solid. Compound (**6a**) (red solid; 200 mg, 27%). ^{1}H NMR ($CDCl_3$, 300 MHz) δ 13.21 (s, 2H), 8.47 (s, 1H), 8.29 (s, 1H), 7.84 (dd, 2H), 7.57–7.48 (m, 4H), 7.24 (d, 2H), 7.00–6.87 (m, 6H), 6.55 (dd, 8H), 6.36 (d, 4H), 5.95 (d, 4H), 3.38 (s, 12H). ^{13}C NMR ($CDCl_3$, 75 MHz) δ 157.2, 151.8, 141.7, 136.7, 136.1, 131.8, 131.4, 128.9, 128.7, 128.1, 126.4, 125.9, 124.6, 122.7, 120.7, 118.2, 111.5, 55.7. MALDI-TOF MS: *m*/*z* calcd for $C_{60}H_{47}N_4O_4$: 887.3519; found: 887.289 $[M + H]^+$. Anal. calcd for $C_{60}H_{46}N_4O_4$: C, 81.24; H, 5.23; N, 6.32. Found: C, 80.66; H, 5.32; N, 6.20.

DPO-OMe (7). Compound **5a** (100 mg, 0.11 mmol) was dissolved in dry CH_2Cl_2 (10 mL) under an argon atmosphere. The reaction mixture was treated with triethylamine (100 μL) for 5 min. Boron trifluoride etherate 48% (200 μL) was added and the mixture was stirred for another 3 h. The reaction mixture was washed with water and brine, dried over Na_2SO_4, and concentrated under reduced pressure. The crude product was purified by silica-gel column chromatography (ethyl acetate/dichloromethane: 1/7) to get the product. Compound **DPO-OMe** (**7**) (red brown solid; 70 mg, 60%). ^{1}H NMR ($CDCl_3$, 300 MHz) δ 8.21 (d, 2H), 7.68 (m, 6H), 7.55 (m, 2H), 7.26 (m, 4H), 6.92–6.82 (m, 8H), 6.70 (d, 4H), 6.45 (d, 4H), 3.66 (s, 12H). ^{13}C NMR ($CDCl_3$, 75 MHz) δ 157.5, 155.9, 153.8, 136.7, 135.5, 132.1, 132.0, 130.5, 130.4, 129.2, 124.6, 123.0, 122.3, 122.3, 122.0, 120.1, 119.4, 110.9, 55.7. HRMS (ESI): *m*/*z* calcd for $C_{58}H_{42}B_2F_4N_4O_5Na^+$: 995.31563; found: 995.31876. Anal. calcd for $C_{58}H_{42}B_2F_4N_4O_5$: C, 71.63; H, 4.35; N, 5.76. Found: C, 71.25; H, 4.16; N, 5.94.

DPA-OMe (8). Compound **6a** (90 mg, 0.10 mmol) was dissolved in dry CH_2Cl_2 (20 mL) under an argon atmosphere. The reaction mixture was treated with triethylamine (250 μL) for 5 min. Boron trifluoride etherate (200 μL) was added and the mixture was stirred for another 3 h. The reaction mixture was washed with water and brine, dried over Na_2SO_4, and concentrated under reduced pressure. The crude product was purified by silica-gel column chromatography (ethyl acetate/dichloromethane: 1/5) to get the product. Compound (**8**) (red brown solid; 40 mg, 40%). ^{1}H NMR ($CDCl_3$, 300 MHz) δ 8.89 (s, 1H), 8.55 (s, 1H), 8.12 (d, 2H), 7.65 (d, 4H), 7.59–7.46 (m, 4H), 7.24–7.16 (m, 4H), 6.74 (t, 8H), 6.42 (d, 4H), 6.28 (d, 4H), 3.59 (s, 12H). ^{13}C NMR ($CDCl_3$, 75 MHz) δ 157.5, 155.5, 140.8, 136.4, 132.7, 132.7, 132.6, 131.5, 131.0, 130.3, 130.0, 129.9, 129.0, 127.2, 124.8, 124.5, 122.0, 122.0, 120.3, 110.8, 55.7. HRMS (ESI): *m*/*z* calcd for $C_{60}H_{44}B_2F_4N_4O_4Na^+$: 1005.33954; found: 1005.33440. Anal. calcd for $C_{60}H_{44}B_2F_4N_4O_4$: C, 73.34; H, 4.51; N, 5.70. Found: C, 73.84; H, 4.80; N, 5.66.

DPO-O (9). To a stirred solution containing **5a** (50 mg, 0.057 mmol) in dry CH_2Cl_2 (5 mL) was added BBr_3 (0.2 mL) at −50 °C under an Ar atmosphere. The reaction mixture was stirred for 3 days allowed to warm up to room temperature and quenched with methanol. The mixture was evaporated and dissolved again with methanol. To the obtained mixture conc. HCl (0.5 mL) was added and heated under reflux for 3 h. The mixture was cooled and neutralized with saturated $NaHCO_3$ aqueous solution and extracted with ethyl acetate. The organic layer was dried over $MgSO_4$, evaporated to dryness. The crude product above was dissolved in dry $CHCl_3$ (10 mL) under an argon atmosphere. $B(OMe)_3$ (100 μL) was added and the mixture was heated to reflux for 3 h. After cooling, the mixture was evaporated to dryness and the residue was purified by column chromatography on silica gel using CH_2Cl_2 as the solvent. Compound **DPO-O** (**9**) (green solid; 15 mg, 31%). ^{1}H NMR (d_6-acetone, 300 MHz) δ 8.32 (dd, 2H), 7.87–7.35 (m, 10H), 7.25–6.80 (m, 14H), 6.72–6.53 (m, 4H). ^{13}C NMR (150 MHz, $CDCl_3$) δ 154.3, 153.9, 153.8, 150.6, 150.2, 134.6, 134.6, 132.2, 132.1, 132.0, 130.8, 129.7, 129.3, 126.0, 125.6, 125.0, 123.5, 122.7, 122.5, 120.3, 120.1, 119.8, 119.7, 119.4, 118.8, 116.1, 116.0. HRMS (MALDI-TOF): *m*/*z* calcd for $C_{54}H_{30}B_2N_4O_5$: 836.2402; found: 836.2464. HRMS (ESI): *m*/*z* calcd for $C_{54}H_{30}B_2N_4O_5Na^+$: 859.23114, found: 859.22896; calcd for $C_{54}H_{30}B_2N_4O_5H^+$: 837.24920, found: 837.24920. Anal. calcd for $C_{54}H_{30}B_2N_4O_5$: C, 77.54; H, 3.62; N, 6.70. Found: C, 77.15; H, 4.16; N, 6.41.

DPA-O (10). The process for the synthesis of compound **(10) DPA-O** is the same as for compound **(9) DPO-O**. Compound (**10**) (green solid; 10 mg, 10%). ^{1}H NMR (300 MHz, $CDCl_3$) δ 8.92 (s, 1H), 8.55 (d, 1H), 8.13 (dd, 2H), 7.69–7.41 (m, 8H), 7.31–7.21 (m, 2H), 7.15–7.05 (m, 2H), 6.49–6.27 (m, 16H). ^{13}C NMR (126 MHz, $CDCl_3$) δ 153.8, 153.6, 153.3, 153.0, 149.7, 149.3, 149.2, 148.8, 134.5, 134.5, 134.4, 134.3, 134.2, 131.0, 130.9, 130.8, 130.7, 130.7, 130.6, 130.5, 129.9, 129.8, 129.7, 129.4, 129.2, 128.7, 128.4, 128.2, 127.7, 127.5, 127.2, 126.4, 126.1, 124.8, 124.4, 124.3, 124.2, 124.1, 124.0, 123.6, 122.7, 119.5, 119.3, 119.2, 118.9, 118.8, 118.6, 118.5, 118.3, 118.2, 115.4, 114.8, 114.2. HRMS (MALDI-TOF): *m*/*z* calcd for $C_{56}H_{32}B_2N_4O_4$: 846.2610; found: 846.2579.

DFT calculations

All density functional theory (DFT) and time dependent density functional theory (TD-DFT) calculations were performed using Gaussian 09[17] at the Université de Sherbrooke with the Mammouth supercomputer supported by Le Réseau Québécois De Calculs Hautes Performances. The DFT geometry optimisations as well as TD-DFT calculations[18–27] were carried out using the B3LYP method. A 6-31g* basis set was applied to all atoms.[28–33] All calculations were carried out in a THF solvent field. The calculated absorption spectra were obtained from GaussSum 2.1.[34]

Instrumentation

UV-Vis spectra were recorded in solutions using a Varian Cary 50 spectrophotometer (1 cm path length quartz cell). NMR spectra were recorded at room temperature using Bruker Avance 300 and Bruker Avance II 600 instruments with the chemical shifts reported as δ in ppm. Accurate mass measurements (HRMS) were carried out using a Bruker microTOF-QTM ESI-TOF mass spectrometer. MALDI-TOF mass spectrometry was carried out using a Bruker Ultraflex II MALDI- TOF mass spectrometer and dithranol as the matrix.

Photophysical studies

Absorption spectra were measured on a Varian Cary 300 Bio UV-vis spectrometer at 298 K and on a Hewlett-Packard 8452A diode array spectrometer with a 0.1 second integration time at 77 K. Steady state fluorescence and excitation spectra were acquired on either a Fluorolog SPEX 1680 equipped with double monochromators for both excitation and emission arms or on an Edinburgh Instruments FLS980 phosphorimeter equipped with single monochromators. All fluorescence spectra were corrected for instrument response. Fluorescence lifetime measurements were made using a GL3300 Nitrogen laser equipped with a high resolution (full width at half-maximum (FWHM) = 1.4 ns) GL302 dye laser from PTI or on the FLS908 phosphorimeter using a 378 nm picosecond pulsed diode laser (FWHM = 78 ps) as an excitation source. Data collection on the FLS980 system is done by time correlated single photon counting (TCSPC).

Quantum yield measurements

Measurements were performed in distillated 2-methyl-tetrahydrofuran (2-MeTHF), and spectrophotometric grade methanol (Aldrich) was used for reference. Quartz cuvettes of 3 mL with a path length of 1 cm equipped with a septum were used, and all solutions were Ar-degassed prior to measurements. Three different measurements (*i.e.*, different solutions) were performed for each quantum yield. The sample concentrations were chosen to obtain an absorbance of about 0.05. The fluorescence quantum yield (Φ_F) measurements were performed with the slit width of 0.5–1.5 nm for both excitation and emission. Relative quantum efficiencies were obtained by comparing the areas under the corrected emission spectra of the sample relative to a known standard, and the following equation was used to calculate the quantum yield:

$$\Phi_{\mathrm{F\,sample}} = (\Phi_{\mathrm{F\,standard}}) \times (I_{\mathrm{sample}}/I_{\mathrm{standard}}) \times (F_{\mathrm{standard}}/F_{\mathrm{sample}}) \times (\eta_{\mathrm{sample}}{}^2/\eta_{\mathrm{standard}}{}^2),$$

where $\Phi_{\mathrm{F(standard)}}$ is the reported quantum yield of the standard, I is the integrated emission spectrum, F is the absorptance ($F = 1-10^{-A}$, where A is the absorbance) at the excitation wavelength, and η is the refractive index of the solvents used. Rhodamine 6G (Φ_F = 0.94 in methanol)[35] and cresyl violet (Φ_F = 0.54 in methanol)[36] were used as standards. In all Φ_F determinations, correction for the solvent refractive index (η) was applied (in 2-MeTHF, η = 1.406; in methanol, η = 1.328).[37]

Results and discussion

Synthesis

The acid-catalyzed condensation of 2-(2-methoxyphenyl)-pyrrole and pentafluorobenzaldehyde in methylene chloride and subsequent oxidation with DDQ afforded the dipyrrin precursor **1** in 77% yield. Deprotection of the phenol moieties with BBr_3 afforded the N_2O_2 dipyrrin **2** in 32% yield. The boron complex **4** was prepared according to a procedure recently reported in the literature upon treatment with $B(OMe)_3$ (Scheme 1).[38]

The synthesis of these bis(dipyrrins) **5a** and **6a** is outlined in Scheme 2. They were obtained in one step in 22–27% yield starting from the dialdehyde linker (*e.g.* antracene dialdehyde or dibenzofuran dialdehyde) and 2-(2-methoxyphenyl)-pyrrole, where the latter reagent was prepared in only one step from commercially available pyrrole and bromoanisole. The ^{1}H NMR spectra of the C_2 symmetric derivative exhibit

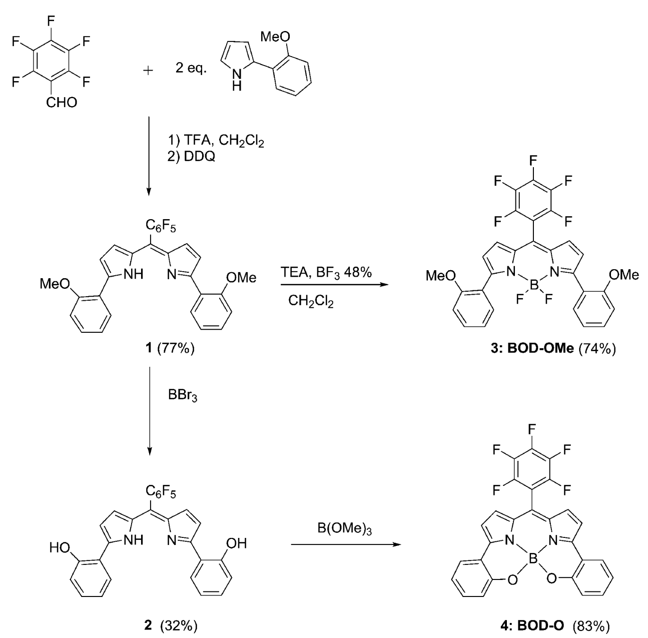

Scheme 1

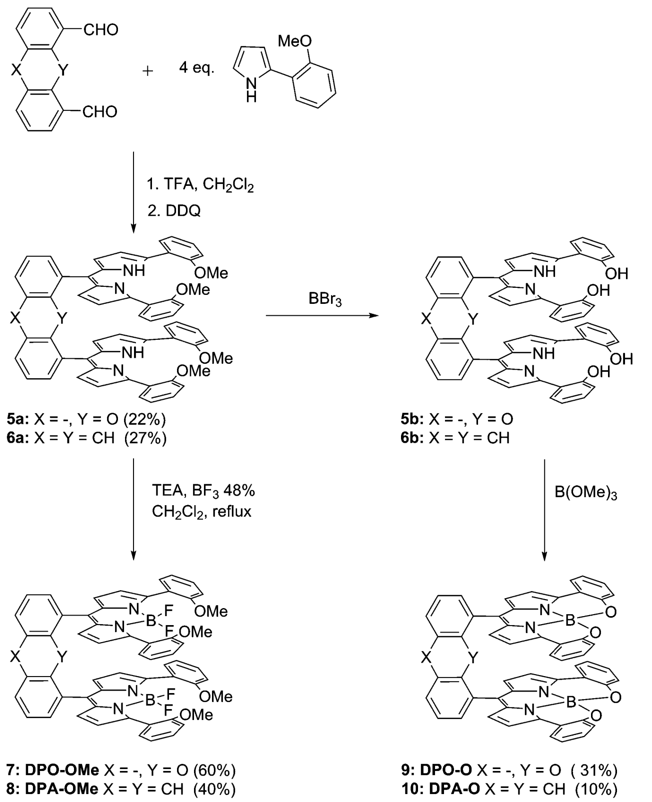

Scheme 2

the characteristic pattern of two *meso*-substituted dipyrrin units cofacially linked by an aromatic bridge (see Experimental section). Peak assignments were made on the basis of chemical shifts, multiplicity, integrations, and spectral intercomparisons with the monodipyrrin derivative as the reference compound. The UV-visible data are reported in the experimental section.

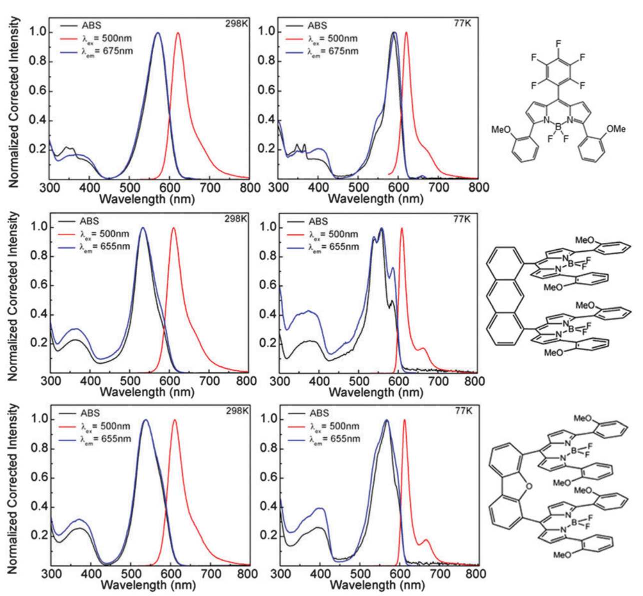

Fig. 3 The absorption (black), excitation (blue) and fluorescence (red) spectra of **BOD-OMe (3)** (top), **DPA-OMe (8)** (middle), and **DPO-OMe (7)** (bottom) in 2MeTHF at 298 K and 77 K. The excitation and monitoring wavelengths are placed in the frames.

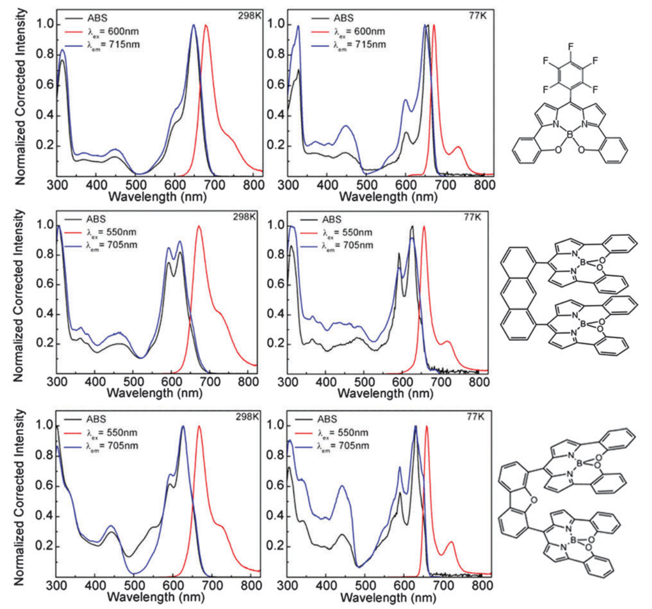

Fig. 4 The absorption (black), excitation (blue) and fluorescence (red) spectra of **BOD-O (4)** (top), **DPA-O (10)** (middle), and **DPO-O (9)** (bottom) in 2MeTHF at 298 and 77 K. The excitation and monitoring wavelengths are placed in the frames.

Table 1 Spectral absorption and emission data of the bis(dipyrrins)

	Absorption (nm) [ε ($\times 10^3$ M^{-1} cm^{-1})]		Emission (nm)	
Compound	298 K	77 K	298 K	77 K
BOD-OMe (3)	284 [21.2] 343 [11.9] 357 [11.3] 570 [47.3]	348 366 555(sh) 588	622 665(sh)	543 621 665(sh)
DPO-OMe (7)	280 [58.7] 370 [24.0] 536 [88.9]	398 569	611 668(sh)	612 667
DPA-OMe (8)	253 [74.5] 280 [40.2] 359 [15.2] 534 [62.9]	376 540 557 584	611 665(sh)	610 664
BOD-O (4)	314 [35.6] 447 [57.5] 607(sh) [16.1] 648 [48.2]	328 448 600 658	679 740(sh)	672 736
DPO-O (9)	303 [62.8] 440 [19.1] 593 [42.5] 625 [71.5]	306 340 442 595 630	667 727(sh)	658 723
DPA-O (10)	254 [99.2] 306 [68.4] 467 [14.0] 593 [52.6] 622 [55.4]	310 482 592 626	672 728(sh)	657 718

Steady state properties

The absorption, excitation and fluorescence spectra of **BOD-OMe (3)**, **DPO-OMe (7)**, **DPA-OMe (8)**, **BOD-O (4)**, **DPO-O (9)**, and **DPA-O (10)** in 2MeTHF are presented in Fig. 3 and 4, and the data are given in Table 1. The assignment for fluorescence is based on the close proximity of the fluorescence and the lowest energy absorption bands, and their lifetimes (below). The excitation spectra superpose well the absorption indicating that the fluorescence arises from the absorbing species (*i.e.* no impurities, or other emitting species). The band shapes of both the absorption and fluorescence spectra are reminiscent of those for BODIPY.[39–41]

The fluorescence lifetimes, τ_F, quantum yields, Φ_F, the radiative k_F (Φ_F/τ_F) and non-radiative, k_{nr} ($(1 - \Phi_F)/\tau_F$), at 298 K are compared in Table 2. Two trends are obvious. The rigidification of the skeleton, for example, on going from **BOD-OMe (3)** to **BOD-O (4)**, increases τ_F by nearly 2-fold. This effect is consistent with the decrease in non-radiative processes associated with the flexibility of the skeleton by removing low-frequency vibration enhancing relaxation (*i.e.* internal conversion). The k_F values decrease by 2 to 3fold on going from the mono(dipyrrin) to the bis(dipyrrins) species. This effect is associated with lower Φ_F values in the bis(dipyrrins) species (excluding the uncertainty for the comparison between the data for **BOD-OMe (3)** and **DPA-OMe (8)**). The k_{nr} value for **DPO-OMe (7)** appears to be unexplainably larger (associated with a lower Φ_F value).

Noteworthy, the fact that τ_F is independent of whether the DPA- and DPO-spacers are used indicates that the two dipyrrin units are not interacting, a behaviour that can easily be addressed as well as demonstrated for the PACMAN systems (see Fig. 1).[15] This behaviour is corroborated using the optimized geometry of the cofacial compounds below. Moreover, the τ_F value (9.45 ns) for **BOD-O (4)** is similar to that

Table 2 Photophysical parameters (τ_F, Φ_F, k_F and k_{nr}) at 298 K (in 2MeTHF)

Compound	λ_{ex}	Φ_F	k_F (10^6 s^{-1})	k_{nr} (10^6 s^{-1})
BOD-OMe (3)	500	0.55	91	75
DPA-OMe (8)	500	0.48	50	54
DPO-OMe (7)	500	0.15	50	280
BOD-O (4)	550	0.49	52	54
DPA-O (10)	550	0.20	15	62
DPO-O (9)	550	0.18	12	56

	298 K		77 K		
Compound	τ_F (ns)	χ^2	τ_F (ns)	χ^2	Monitoring wavelength (nm)
BOD-OMe (3)	6.04 ± 0.05	1.085	5.94 ± 0.05	1.107	625
DPA-OMe (8)	9.63 ± 0.05	1.089	9.56 ± 0.06	1.046	610
DPO-OMe (7)	3.03 ± 0.05	1.004	9.68 ± 0.10	1.044	610
BOD-O (4)	9.45 ± 0.05	1.118	10.47 ± 0.05	1.074	680
DPA-O (10)	12.9 ± 0.05	1.050	17.6 ± 0.05	1.033	665
DPO-O (9)	14.7 ± 0.10	1.024	18.2 ± 0.05	1.027	665

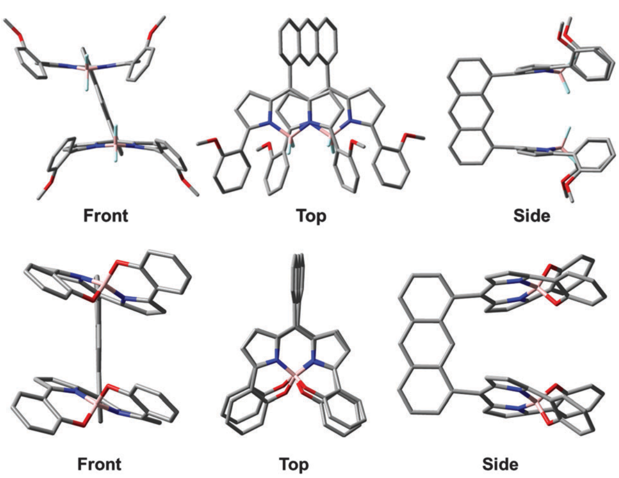

Fig. 5 Optimized geometries (DFT, B3LYP) for **DPA-OMe (8)** (top) and **DPA-O (10)** (bottom).

Table 3 Selected structural parameters

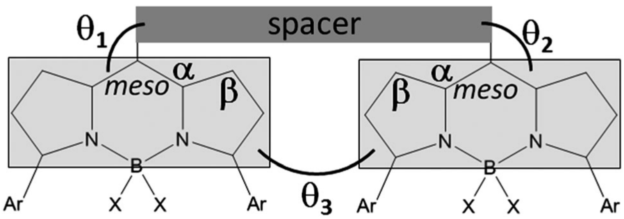

	B···B (Å)	$C_{meso}\cdots C_{meso}$ (Å)	X···X (Å)	Shortest dist. (Å)	$\theta_1 = \theta_2$ (°)	θ_3 (°)
DPO-OMe (7)	6.96	5.62	5.12	5.27 (*meso*-β)	62.3	26.7
DPA-OMe (8)	5.31	5.17	3.06	5.05 (*meso*-α)	70.6	5.63
DPO-O (9)	7.43	5.65	6.49	4.98 (*meso*-β)	59.6	28.9
DPA-O (10)	6.12	5.26	4.45	4.49 (*meso*-α)	68.4	16.9

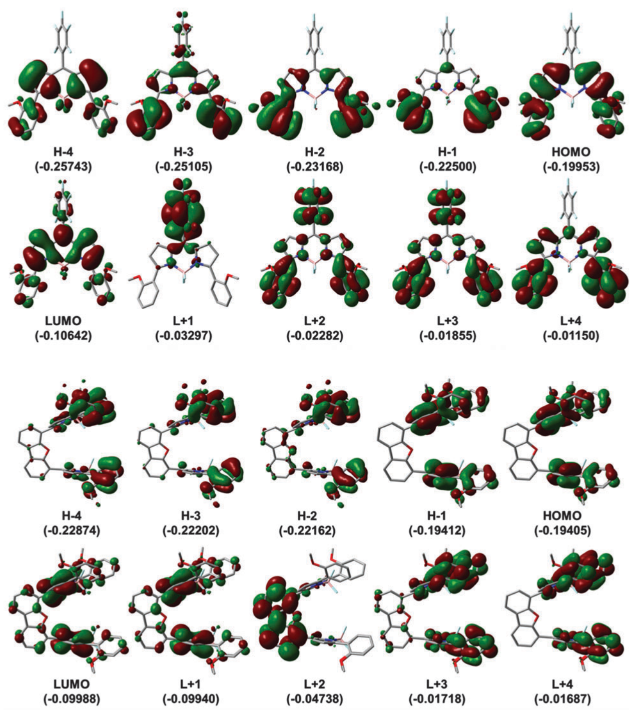

Fig. 6 Representations of the frontier MOs for **BOD-OMe (3)** (top) and **DPO-OMe (7)** (bottom) as representative examples (see ESI,† for the other compounds). The energies are in a.u.

reported for similar (and only example) mono-*o*-chelated bis-(dipyrrin) (9.6 ns).[42]

Optimized geometry

In the absence of X-ray structures, the geometry of the cofacial dimers has been addressed using DFT computations. Representative examples of optimized geometries are provided in Fig. 5 (see ESI,† for **DPO-OMe (7)** and **DPO-O (9)**). The geometry of bis(dipyrrin)s is best described as slipped dimers as defined by the dihedral angles θ_1 and θ_2 made by the average planes of the dipyrrin and spacer units (Table 3). These dimers further exhibit an "open mouth" geometry from the non-nil dihedral angle θ_3. The fact that θ_3(DPA) < θ_3(DPO) is predictable due to the intrinsic geometry of the spacer.

Concurrently, both θ_1 and θ_2 are similar for both spacers (DPA $\sim$ 70°; DPO $\sim$ 61°). The slight difference is related to the β-hydrogen atoms with the spacer. The computed $C_{meso}\cdots C_{meso}$ separations ($\sim$5.2 Å for DPA and $\sim$5.6 Å for DPO) compare favourably to those experimentally measured by X-ray crystallography (respectively 4.94 Å and 5.53 Å in the PACMAN series; Fig. 1).[14] Based on the shortest calculated atom-atom separations between the two chromophores, the computed geometry does not result from any contact as the evaluated separations exceed the sum of van der Waals. The closest distance is 3.06 Å for F···F in **DPA-OMe (8)** (the van der Waals radius for F is 1.35 Å).[43] Other distances of 4.13 Å (F–N) in **DPA-O (10)** and 5.39 Å (F–Cα) in **DPO-OMe (7)** are also noted but clearly these values are larger than the sum of the van der Waals radii. It is concluded that the geometry is not limited by inter-atomic contacts inside the "sandwich" area of the cofacial dimers, but rather by steric limitations between the β-protons and the spacer. There is no computational evidence for through space inter-dipyrrin interactions.

Excited state description

The nature of the excited states was addressed by DFT and TDDFT. In all cases the atomic contributions are π-orbitals arising from

Table 4 Percent distribution of the molecular orbitals over selected molecular fragments of **DPO-OMe (7)**

Fragment	H−4	H−3	H−2	H−1	HOMO
DPO	2.9	2.1	5.5	3.6	2.1
Dipyrrin 1	**48.6**	**48.9**	**47.3**	**47.9**	**49.2**
Dipyrrin 2	**48.4**	**49.0**	**47.2**	**48.5**	**48.7**

Fragment	LUMO	L+1	L+2	L+3	L+4
DPO	10.5	8.7	**89.7**	5.2	2.6
Dipyrrin 1	**44.8**	**45.6**	5.2	**47.4**	**48.6**
Dipyrrin 2	**44.7**	**45.7**	5.2	**47.4**	**48.7**

Table 5 Computed oscillator strengths (*F*), positions of the first electronic transitions and major contributions of **BOD-OMe (3)**, **DPA-OMe (8)**, **DPO-OMe (7)**, **BOD-O (4)**, **DPA-O (10)** and **DPO-O (9)**[a]

Compound	λ^b (nm)	*F*	Major contributions (%)
BOD-OMe (3)			
1	533.5 (588)	0.6403	HOMO → LUMO (96)
2	452.8	0.0826	H−1 → LUMO (99)
3	421.0	0.0845	H−2 → LUMO (95)
DPA-OMe (8)			
1	574.3 (569)	0.0129	H−1 → L+1 (20), HOMO → LUMO (74)
2	572.4	0.0078	H−1 → LUMO (31), HOMO → L+1 (63)
3	537.7	0.0180	H−2 → LUMO (18), H−1 → L+1 (71), HOMO → LUMO (10)
4	532.8	0.2454	H−2 → L+1 (47), H−1 → LUMO (44)
DPO-OMe (7)			
1	565.0 (584)	0.0005	H−1 → LUMO (43), HOMO → LUMO (11), HOMO → L+1 (37)
2	565.0	0.0022	H−1 → LUMO (11), H−1 → L+1 (37), HOMO → LUMO (43)
3	534.9	0.0213	H−1 → LUMO (45), HOMO → L+1 (53)
4	525.0	1.1673	H−1 → L+1 (53), HOMO → LUMO (45)
BOD-O (4)			
1	580.8 (658)	0.3993	HOMO → LUMO (99)
2	480.9	0.1187	H−1 → LUMO (98)
3	415.8	0.0594	H−2 → LUMO (98)
DPA-O (10)			
1	608.8 (630)	0.0137	H−1 → L+1 (20), HOMO → LUMO (79)
2	605.8	0.0038	H−1 → LUMO (48), HOMO → L+1 (51)
3	572.3	0.0057	H−1 → L+1 (79), HOMO → LUMO (19)
4	561.6	0.4780	H−2 → L+1 (16), H−1 → LUMO (46), HOMO → L+1 (37)
DPO-O (9)			
1	597.5 (626)	0.0001	H−1 → L+1 (38), HOMO → LUMO (62)
2	597.2	0.0018	H−1 → LUMO (55), HOMO → L+1 (45)
3	571.3	0.0066	H−1 → L+1 (62), HOMO → LUMO (37)
4	559.1	0.7257	H−1 → LUMO (45), HOMO → L+1 (54)

[a] For the 75 first electronic transitions, see ESI. H = HOMO, L = LUMO. [b] The values in parentheses are those experimentally measured at 77 K from Table 1.

various chromophore segments providing evidence for low-energy $\pi \rightarrow \pi^*$ electronic transitions (Fig. 6 and ESI,†). A clear plane of symmetry between the right and left sides is also observed. An examination of the HOMO → LUMO transition also suggests the presence of a minor charge transfer contribution (from the OC_6H_4 groups to the central dipyrrin unit). Interestingly in all cofacial chromophores, an equivalent contribution of the π-systems is computed (Table 4). The absence of or very modest atomic contributions arising from the spacer for the frontier MOs (H−1, HOMO, LUMO, L+1) suggests that in all cases π-conjugation is either minimal or negligible. This conclusion is corroborated by the absence of significant (red) shifts of absorption and fluorescence bands (Fig. 3 and 4).

Moreover, the absence of band broadening in the absorption and fluorescence spectra indicates the absence of MO coupling between the two dipyrrins. These observations indicate again that the two chromophores act independently, which is fully consistent with the conclusion drawn with the comparison of the photophysical parameters. In brief, the atomic contributions calculated for both chromophores are due to symmetry, and not due to coupling or conjugation.

In order to support the current ππ* assignment and the absence of inter-dipyrrin interactions, the positions of the electronic transitions has been calculated (TDDFT; Table 5 and Fig. 7). The calculated lowest energy electronic transitions (*i.e.* 0–0 peaks) are placed in the 533–565 and 580–609 nm range for the **BOD-OMe**, **DPA-OMe** and **DPO-OMe**, and the **BOD-OMe**, **DPA-O** and **DPO-O** series, respectively. This red-shift on going from the first to the second series is consistent with the experimental observations (Table 1). The comparison between the calculated and experimental positions is good for the bis(dipyrrin) compounds with discrepancies of only 5–28 nm. Note that the selected data are those measured at 77 K because the spectra are more resolved allowing a better evaluation of the positions of the 0–0 components. However, this comparison is worse for the mono-pyrrin species (55–78 nm difference) but yet not shocking. By (arbitrarily) assigning a thickness of 500 cm^{-1} to each calculated transition (in blue, Fig. 7), theoretical spectra are thus generated (in black). Despite the fact that this approach does not take into account the contribution of vibrational progression, the comparison between the generated spectra (Fig. 7) with the experimental ones (Fig. 3, 298 K, left) is good.

The three first computed lowest energy transitions for the two mono-pyrrins **BOD-OMe (3)** and **BOD-O (4)** exhibit almost pure contributions of the H−2 → LUMO, H−1 → LUMO and HOMO → LUMO (Table 5). Conversely, the bis(dipyrrin)s exhibit mixed contributions. This computational observation is a natural predictable consequence of the symmetry in the atomic contributions (as illustrated in Table 4), and of the close proximity in MO energy between the HOMO and the H−1, and between the LUMO and the L+1 (for instance see Fig. 6). Thus, the computed data confirm that the nature of the mono- and bis(dipyrrins) fluorescent states is ππ*. A little charge transfer character from the flanking aromatic OC_6H_4 groups to the central dipyrrin unit is also computed.

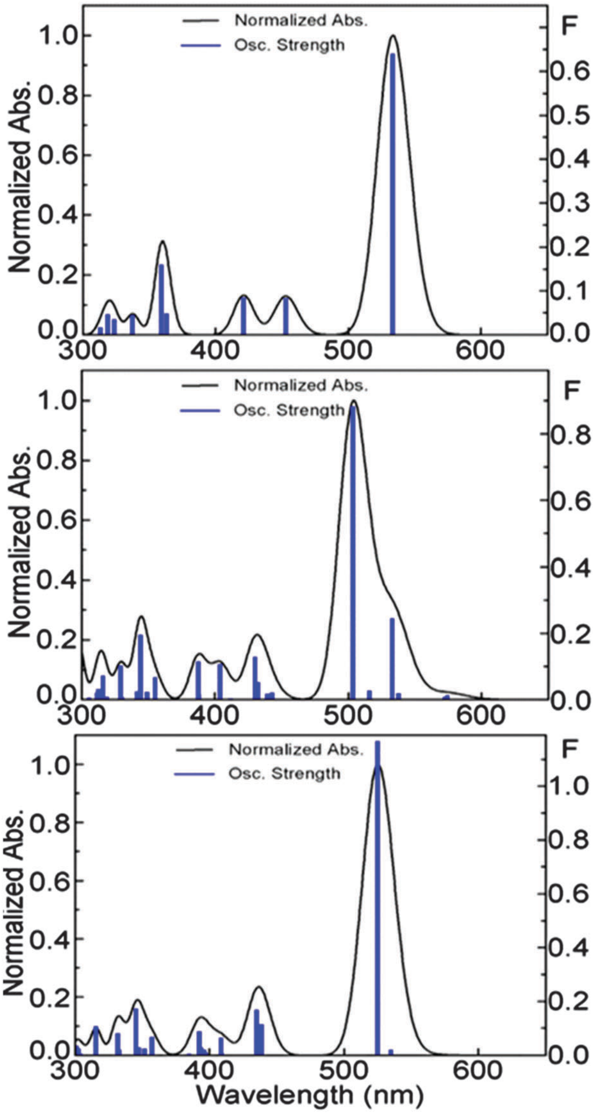

Fig. 7 Graphs reporting the computed oscillator strength (*F*) as a function of the calculated positions of the first 75 electronic transitions for **BOD-OMe (3)** (top), **DPA-OMe (8)** (middle) and **DPO-OMe (7)** (bottom). See the ESI,† for **BOD-O (4)**, **DPA-O (10)** and **DPO-O (9)**.

Quenching analysis

Fluorescence quenching experiments using C_{60} as an electron acceptor were carried out on all compounds. Upon the addition of C_{60}, the fluorescence intensity of the dipyrrin species in 1,2-dichlorobenzene undergoes a decrease (see **BOD-OMe** in Fig. 9 as a representative example). The Stern–Volmer (left) plots report these intensity decreases ($\Phi_F^0/\Phi_F = F_0/F$; *i.e.* relative intensity in the absence over in the presence of quencher) with $[C_{60}]$, but not for the lifetime (τ_0/τ; *i.e.* relative dipyrrin fluorescence lifetime in the absence over in the presence of a quencher) indicating the presence of static quenching:

$$\underset{\text{fluorescent}}{{}^1\text{pyrrin}^* + C_{60}} \leftrightarrow \underset{\text{static complex}}{[{}^1\text{pyrrin}^* \cdots C_{60}]} \rightarrow \underset{\text{not emissive}}{[\text{pyrrin}^{\bullet+} \cdots C_{60}{}^{\bullet-}]} \quad (1)$$

Although it is meant to analyze dynamic quenching (diffusional), for comparison purposes the quenching constant

Table 6 Stern–Volmer and modified Stern–Volmer analyses for BODIPY dyads

	K_{SV} (10^3 M^{-1})			R^2	
Compound	Stern–Volmer	Modified S–V[a]	k_Q (10^8 M^{-1} s^{-1})	Stern–Volmer	Modified S–V[a]
BOD-OMe (3)	1.37	1.14	1.89	0.990	0.968
DPA-OMe (8)	1.53	1.59	1.65	0.995	0.998
DPO-OMe (7)	1.26	1.42	4.69	0.992	0.983
BOD-O (4)	0.85	0.89	0.94	0.983	0.978
DPA-O (10)	1.48	1.38	1.07	0.992	0.977
DPO-O (9)	0.90	1.01	0.69	0.991	0.955

[a] Intercept of the regression curves was forced to 1 (*i.e.* assuming that $f = 1$).

extracted from the Stern–Volmer analysis, K_{SV} (from the relationship $(F_0/F) = K_{SV}\cdot[C_{60}] + 1$) was determined (Table 6). For static quenching, the relationship is modified and becomes $F_0/(F_0 - F) = 1/(f\cdot K_{SV}\cdot[C_{60}]) + 1/f$, where f (normally extracted from the intercept) is the fraction of chromophores that are accessible (so $f = 1$).[44] The K_{SV} constants are given by $k_q\cdot\tau_0$ where k_q is the bimolecular quenching rate constant. The k_q values were obtained from the K_{SV} data measured from the modified Stern–Volmer approach. The extracted values are considered fast indicating that the process is definitely diffusion controlled and that these values for the **BOD-OMe**, **DPA-OMe** and **DPO-OMe** series are larger than those for their corresponding **BOD-O**, **DPA-O** and **DPO-O**.[44]

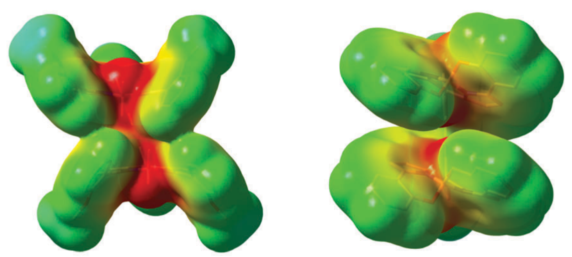

DPA-OMe (8) **DPA-O (10)**

Fig. 8 Electronic density map (DFT) for **DPA-OMe (8)** and **DPA-O (10)**. The red and blue areas are respectively the electron rich and poor segments of the molecule. See the ESI,† for the two DPO-bis(dipyrrins).

Knowing that there is not enough space inside the "mouth" of the bis(dipyrrins) based on the optimized geometries, these static complexes must be formed *via* outside contacts.

This conclusion is clear when comparing the k_Q values between **BOD-OMe (3)** and **DPA-OMe (8)**, and between **BOD-O (4)** and **DPA-O (10)** as they are nearly the same. The "outside" interactions are also evidenced by the electronic density map (Fig. 8) where the electron poor areas will interact more favorably with the electron rich C_{60}.

It is unclear whether the larger k_Q values for the **BOD-OMe**, **DPA-OMe** and **DPO-OMe** series are larger because the binding constants between bis(dipyrrin)s and C_{60} are larger. However, because of the flexibility of $MeOC_6H_4$ groups, these latter aromatics can adapt through rotations to favour ππ-interactions. This is not the case for the other series **BOD-O**, **DPA-O** and **DPO-O**. This possibility does not exclude the possibility that the excited state driving forces for electron transfers are simply larger due to the presence of the electron donating OMe groups for the former series. So, no firm conclusion can be provided at this time on this trend.

Conclusions

Bis(dipyrrins) were easily prepared using standard procedures and proved to be useful to demonstrate the absence of inter-dipyrrin interactions. Indeed, spectroscopy and computer modeling allow for this evidence. The calculated inter-atomic distances are systematically larger than the sum of van der Waals radii and unambiguously demonstrate that, in fact, the rigidity of the DPO- and DPA-spacers induces this effect. This conclusion is perfectly in line with the reported absence of triplet–triplet energy transfers in the cofacial hetero-bis(porphyrin) systems held by DPA and DPO.[14] Indeed, the triplet–triplet energy transfer is dominated by the Dexter mechanism[45] (double electron exchange) and the absence of significant orbital contacts makes this process very difficult, not to say inexistent. The bimolecular quenching of cofacial bis(dipyrrins) with the strong electron acceptor C_{60} indicates that diffusion-controlled quenching occurs from outside contacts between the pairs. Knowing that one of the cofacial dipyrrin units can act as a shield protecting

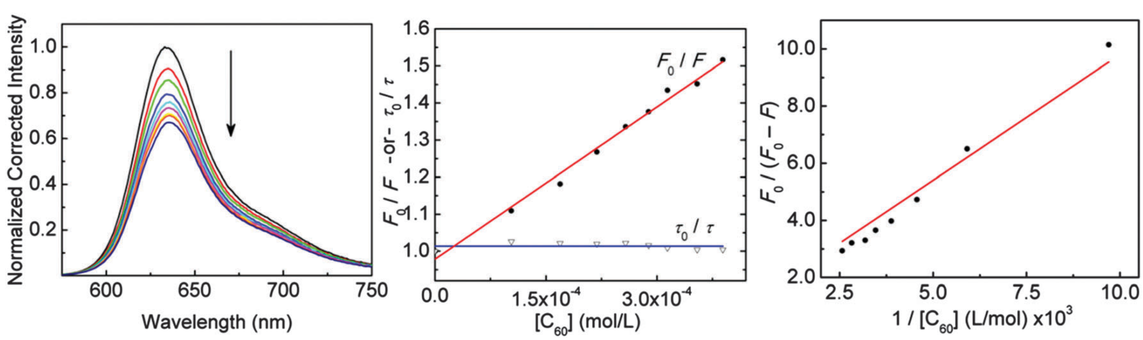

Fig. 9 Left: Evolution of fluorescence spectra of **BOD-OMe (3)** in 1,2-dichlorobenzene upon the addition of C_{60}. Middle: Stern–Volmer analysis of fluorescence quenching of **BOD-OMe** by C_{60} in 1,2-dichlorobenzene. Right: Modified Stern–Volmer analysis. See the ESI,† for the five other compounds. The C_{60} concentration was increased from 0 to 18.5 equivalents.

one face of the excited other dipyrrin, the similarity in the bimolecular quenching rate constants between the mono- and bis(dipyrrins) (except for one unexplained case) suggests that nonetheless the static complex must be close to both chromophores at the same time. The conclusion drawn from this study indicates that there is no real advantage to use the cofacial structure for the design of photonic devices such as photocells, but does not exclude that in the solid state (*i.e.* bulk heterojunction-type cell) this situation would be different due to the formation of aggregates.

Acknowledgements

This research was supported by the Natural Sciences and Engineering Research Council of Canada (NSERC), le ''Fonds Québécois de la Recherche sur la Nature et les Technologies (FQRNT)'' the ''Centre d'Etudes des Matériaux Optiques et Photoniques de l'Université de Sherbrooke (CEMOPUS)''. The ''Centre National de la Recherche Scientifique'' (ICMUB, UMR CNRS 6302) is gratefully thanked for financial support. Yi Chang also gratefully acknowledges the ''Région Bourgogne'' and CNRS for a post-doctoral fellowship. Support was provided by the CNRS, the ''Université de Bourgogne'' and the ''Conseil Régional de Bourgogne'' through the 3MIM integrated project (''Marquage de Molécules par les Métaux pour l'Imagerie Médicale''). We are also thankful to the ''Consulat Général de France à Québec'' for a ''Samuel de Champlain'' grant.

Notes and references

1 S. A. Baudron, *Dalton Trans.*, 2013, **42**, 7498–7509.
2 N. Boens, B. Verbelen and W. Dehaen, *Eur. J. Org. Chem.*, 2015, 6577–6595.
3 Y. Ding, Y. Tang, W. Zhu and Y. Xie, *Chem. Soc. Rev.*, 2015, **44**, 1101–1112.
4 R. Sakamoto, T. Iwashima, M. Tsuchiya, R. Toyoda, R. Matsuoka, J. F. Kogel, S. Kusaka, K. Hoshiko, T. Yagi, T. Nagayama and H. Nishihara, *J. Mater. Chem. A*, 2015, **3**, 15357–15371.
5 S. A. Baudron, *CrystEngComm*, 2010, **12**, 2288–2295.
6 R. Sakamoto, S. Kusaka, M. Hayashi, M. Nishikawa and H. Nishihara, *Molecules*, 2013, **18**, 4091–4119.
7 T. E. Wood and A. Thompson, *Chem. Rev.*, 2007, **107**, 1831–1861.
8 E. V. Antina, R. T. Kuznetsova, L. A. Antina, G. B. Guseva, N. A. Dudina, A. I. V'Yugin and A. V. Solomonov, *Dyes Pigm.*, 2015, **113**, 664–674.
9 P. D. Harvey, C. Stern, C. P. Gros and R. Guilard, *J. Inorg. Biochem.*, 2008, **102**, 395–405.
10 P. D. Harvey, C. Stern, C. P. Gros and R. Guilard, *J. Porphyrins Phthalocyanines*, 2010, **14**, 55–63.
11 P. D. Harvey, *Can. J. Chem.*, 2014, **92**, 355–368.
12 P. D. Harvey, M. A. Filatov and R. Guilard, *J. Porphyrins Phthalocyanines*, 2011, **15**, 1150–1171.
13 P. D. Harvey, C. Stern and R. Guilard, in *Handbook of Porphyrin Science With Applications to Chemistry, Physics, Materials Science, Engineering, Biology and Medicine*, ed. K. M. Kadish, K. M. Smith and R. Guilard, World Scientific Publishing, Singapore, 2011, pp. 1–179.
14 S. Faure, C. Stern, R. Guilard and P. D. Harvey, *J. Am. Chem. Soc.*, 2004, **126**, 1253–1261.
15 F. Bolze, C. P. Gros, M. Drouin, E. Espinosa, P. D. Harvey and R. Guilard, *J. Organomet. Chem.*, 2002, 89–97.
16 S. Faure, C. Stern, E. Espinosa, R. Guilard and P. D. Harvey, *Chem. – Eur. J.*, 2005, **11**, 3469–3481.
17 M. J. Frisch, G. W. Trucks, H. B. Schlegel, G. E. Scuseria, M. A. Robb, J. R. Cheeseman, J. A. Montgomery, Jr., T. Vreven, K. N. Kudin, J. C. Burant, J. M. Millam, S. S. Iyengar, J. Tomasi, V. Barone, B. Mennucci, M. Cossi, G. Scalmani, N. Rega, G. A. Petersson, H. Nakatsuji, M. Hada, M. Ehara, K. Toyota, R. Fukuda, J. Hasegawa, M. Ishida, T. Nakajima, Y. Honda, O. Kitao, H. Nakai, M. Klene, X. Li, J. E. Knox, H. P. Hratchian, J. B. Cross, V. Bakken, C. Adamo, J. Jaramillo, R. Gomperts, R. E. Stratmann, O. Yazyev, A. J. Austin, R. Cammi, C. Pomelli, J. W. Ochterski, P. Y. Ayala, K. Morokuma, G. A. Voth, P. Salvador, J. J. Dannenberg, V. G. Zakrzewski, S. Dapprich, A. D. Daniels, M. C. Strain, O. Farkas, D. K. Malick, A. D. Rabuck, K. Raghavachari, J. B. Foresman, J. V. Ortiz, Q. Cui, A. G. Baboul, S. Clifford, J. Cioslowski, B. B. Stefanov, G. Liu, A. Liashenko, P. Piskorz, I. Komaromi, R. L. Martin, D. J. Fox, T. Keith, M. A. Al-Laham, C. Y. Peng, A. Nanayakkara, M. Challacombe, P. M. W. Gill, B. Johnson, W. Chen, M. W. Wong, C. Gonzalez and J. A. Pople, *Gaussian 03 (Revision C.02)*, Gaussian, Inc., Wallingford CT, 2004.
18 R. Bauernschmitt and R. Ahlrichs, *Chem. Phys. Lett.*, 1996, **256**, 454–464.
19 A. D. Becke, *J. Chem. Phys.*, 1993, **98**, 5648–5652.
20 M. E. Casida, C. Jamorski, K. C. Casida and D. R. Salahub, *J. Chem. Phys.*, 1998, **108**, 4439–4449.
21 P. Hohenberg and W. Kohn, *Phys. Rev.*, 1964, **136**, B864–871.
22 P. Hohenberg and W. Kohn, *J. Phys. Rev.*, 1965, **140**, A1133–1138.
23 C. Lee, W. Yang and R. G. Parr, *Phys. Rev. B: Condens. Matter Mater. Phys.*, 1988, **37**, 785–789.
24 B. Miehlich, A. Savin, H. Stoll and H. Preuss, *Chem. Phys. Lett.*, 1989, **157**, 200–206.
25 R. G. Parr and W. Yang, *Density-functional theory of atoms and molecules*, Oxford Univ. Press, Oxford, 1989.
26 D. R. Salahub and M. C. Zerner, *The Challenge of d and f Electrons*, Amer. Chem. Soc., Washington, D.C., 1989.
27 R. E. Stratmann, G. E. Scuseria and M. J. Frisch, *J. Chem. Phys.*, 1998, **109**, 8218–8224.
28 J. S. Binkley, J. A. Pople and W. J. Hehre, *J. Am. Chem. Soc.*, 1980, **102**, 939–947.
29 K. D. Dobbs and W. J. Hehre, *J. Comput. Chem.*, 1986, **7**, 359–378.
30 K. D. Dobbs and W. J. Hehre, *J. Comput. Chem.*, 1987, **8**, 861–879.
31 K. D. Dobbs and W. J. Hehre, *J. Comput. Chem.*, 1987, **8**, 880–893.
32 M. S. Gordon, J. S. Binkley, J. A. Pople, W. J. Pietro and W. J. Hehre, *J. Am. Chem. Soc.*, 1982, **104**, 2797–2803.
33 W. J. Pietro, M. M. Francl, W. J. Hehre, D. J. Defrees, J. A. Pople and J. S. Binkley, *J. Am. Chem. Soc.*, 1982, **104**, 5039–5048.

34 N. M. O'Boyle, A. L. Tenderholt and K. M. Langner, *J. Comput. Chem.*, 2008, **29**, 839–845.
35 W. Baumler and A. Penzkofer, *Chem. Phys.*, 1990, **140**, 75–97.
36 D. Magde, J. H. Brannon, T. L. Cremers and J. Olmsted, III, *J. Phys. Chem.*, 1979, **83**, 696–699.
37 D. R. Lide, *Handbook of Chemistry and Physics*, Chemical Rubber Publishing Co, Berlin, 1957.
38 C. Ikeda, S. Ueda and T. Nabeshima, *Chem. Commun.*, 2009, 2544–2546.
39 B. Brizet, N. Desbois, A. Bonnot, A. Langlois, A. Dubois, J.-M. Barbe, C. P. Gros, C. Goze, F. Denat and P. D. Harvey, *Inorg. Chem.*, 2014, **53**, 3392–3403.
40 B. Brizet, A. Eggenspiller, C. P. Gros, J.-M. Barbe, C. Goze, F. Denat and P. D. Harvey, *J. Org. Chem.*, 2012, **77**, 3646–3650.
41 H.-J. Xu, A. Bonnot, P.-L. Karsenti, A. Langlois, M. Abdelhammed, J.-M. Barbe, C. P. Gros and P. D. Harvey, *Dalton Trans.*, 2014, **43**, 8219–8229.
42 Y. Tomimori, T. Okujima, T. Yano, S. Mori and N. Ono, *Tetrahedron*, 2011, **67**, 3187–3193.
43 F. A. Cotton, G. Wilkinson and P. L. Gaus, *Basic Inorganic Chemistry*, Wiley, New-York, 3rd edn, 1995.
44 J. R. Lakowicz, *Principles of Fluorescence Spectroscopy*, Springer: Berlin, 3rd edn, 2006.
45 D. L. Dexter, *J. Chem. Phys.*, 1953, **21**, 836–850.